Realization of a Cross-Linked Chiral Ladder with Neutral Fermions in a 1D Optical Lattice by Orbital-Momentum Coupling

Jin Hyoun Kang, Jeong Ho Han, and Y. Shin*
Department of Physics and Astronomy, and Institute of Applied Physics, Seoul National University, Seoul 08826, Korea and Center for Correlated Electron Systems, Institute for Basic Science, Seoul 08826, Korea

(Received 3 July 2018; published 12 October 2018)

We report the experimental realization of a cross-linked chiral ladder with ultracold fermionic atoms in a 1D optical lattice. In the ladder, the legs are formed by the orbital states of the optical lattice and the complex interleg links are generated by the orbital-changing Raman transitions that are driven by a moving lattice potential superimposed onto the optical lattice. The effective magnetic flux per ladder plaquette is tuned by the spatial periodicity of the moving lattice, and the chiral currents are observed from the asymmetric momentum distributions of the orbitals. The effect of the complex cross-links is demonstrated in quench dynamics by measuring the momentum dependence of the interorbital coupling strength. We discuss the topological phase transition of the chiral ladder system for the variations of the complex cross-links.

DOI: 10.1103/PhysRevLett.121.150403

Topological states of matter represent one of the frontiers of modern condensed matter physics [1,2]. Featuring tunable artificial gauge fields and spin-orbit coupling [3], ultracold atoms in optical lattices provide a versatile platform to realize topological states and study their phase transitions in a clean and well-controlled manner [4,5]. The Hofstadter-Harper model, which is the paradigmatic example of a topological Chern insulator, was realized in 2D optical lattices using laser-assisted tunneling effects [6,7]; the Haldane model was demonstrated in a hexagonal optical lattice by activating complex next-nearest-neighbor (NNN) hopping with lattice shaking [8]. The high tunability of the experimental parameters may enable one to explore a broad range of topological states even beyond the conventional Altland-Zirnbauer classification [9,10].

In recent optical-lattice experiments, an interesting framework was introduced to realize chiral ladder systems with 1D optical lattices, where the internal atomic degrees of freedom, such as hyperfine spin, are taken as a finite synthetic dimension and an artificial gauge field is engineered by laser-induced couplings between the internal states [11,12]. The synthetic ladder systems are highlighted by their edges, which are intrinsically sharp and can be detected by internal-state-selective imaging, thus allowing direct observation of the chiral edge currents in the systems [13–15]. Ladders with complex hopping amplitudes have been discussed as a minimal model for 1D topological matter [16] and also as a quasi-1D version of the Hofstadter problem for studying the edge-mode states in 2D topological insulators [17]. In particular, it is well recognized that NNN hopping, i.e., diagonal cross-links between the legs, are responsible for the emergence of topologically nontrivial phases in the ladder system [17–19]. Therefore, extensive control of the complex interleg links is highly desirable in synthetic ladder experiments.

In this Letter, we report the experimental demonstration of a synthetic ladder scheme using the orbital degree of freedom of the optical lattice system. The legs of the ladder are formed by the orbital states, and the interleg hoppings are generated by orbital-changing two-photon Raman transitions that are resonantly driven by a moving lattice potential. The complex hopping amplitude is spatially modulated, giving rise to an effective magnetic flux Φ per ladder plaquette, which we demonstrate by observing the corresponding chiral currents of the orbital states. The key feature of our orbital-based ladder system is that the cross interleg links are significantly strong due to the favorable condition for the spatial overlap of the orbital wave functions. The complex cross-link effect is manifested in the momentum dependence of the interorbital coupling strength, which we directly demonstrate via momentum-resolved analysis of the quench dynamics of the ladder system. Finally, we discuss the topological phase transition, which can occur in the system by further controlling the cross-link, possibly via tailoring the orbital wave functions. Our results present a new perspective for studies of topological phases with optical lattice systems using the orbital degree of freedom [20–22].

We consider a system of noninteracting spinless fermions in a 1D lattice potential $V(x) = V_L \cos^2(k_L x)$, where the fermions are perturbed by a moving lattice potential, $\delta V(x,t) = V_R \cos^2\{k_R x - [(\omega t)/2]\}$ [Fig. 1(a)]. The Hilbert space of the system is spanned by the Wannier states $\{|j,\alpha\rangle\}$ of the stationary lattice potential, where j and α are the indices for the lattice site and orbital, respectively. Regarding the orbital degree of freedom as a virtual dimension orthogonal to the real lattice dimension, the system can be viewed as a

synthetic 2D lattice system that has a sharp edge formed by the s orbital, as depicted in Fig. 1(b). When the modulation frequency ω of the moving lattice is close to a band gap, orbital-changing Raman transitions are resonantly driven, realizing hoppings for the synthetic dimension. The moving lattice is a resulting form of two Raman laser beams with different frequencies.

In a multiband tight-binding description [23], using the rotating wave approximation, the system's Hamiltonian is given by [24]

$$H=\sum_{j,\alpha}\Big[(\epsilon_\alpha-\alpha\hbar\omega)c^\dagger_{j,\alpha}c_{j,\alpha}+[(-1)^{\alpha+1}t^r_\alpha c^\dagger_{j,\alpha}c_{j+1,\alpha}+\text{H.c.}] +\frac{1}{2}(t^s_\alpha e^{-i\varphi j}c^\dagger_{j,\alpha}c_{j,\alpha+1}+\text{H.c.}) +\frac{1}{2}\sum_{l=\pm1}(t^d_\alpha e^{-i(\varphi j+\varphi'_\alpha l)}c^\dagger_{j,\alpha}c_{j+l,\alpha+1}+\text{H.c.})\Big], \quad (1)$$

where $c_{j,\alpha}$ ($c^\dagger_{j,\alpha}$) is the annihilation (creation) operator for a fermion on site (j,α). The first term is the on-site energy in the rotating frame, the second and third terms describe the nearest-neighbor hopping along the real and synthetic directions, respectively, and the fourth term represents the NNN, diagonal hopping in the 2D rectangular lattice. The position-dependent complex phase factor $e^{i\varphi j}$ for orbital-changing hopping results from the spatial variation of the phase of the moving lattice potential and $\varphi=2\pi(k_R/k_L)$. When a fermion hops around a unit cell, it acquires a net phase of $\Phi=\varphi+\pi$, which can be interpreted as a magnetic flux piercing through the lattice plaquette [6,7]. Here the phase of π in Φ is due to parity inversion between two intermediate orbitals. Taking into account the additional complex phase factor $e^{i\varphi'_\alpha l}$ for diagonal hopping, a subplaquette flux distribution can be assigned, as shown in Fig. 1(b), where $\phi_\alpha=\varphi/2-\varphi'_\alpha$. For given orbital wave functions, t^s_α/t^d_α and φ'_α are determined to be functions of k_R/k_L [Figs. 1(c) and 1(d)].

Our experiment starts with the preparation of a spin-polarized degenerate Fermi gas of ^{173}Yb atoms in the $|F,m_F\rangle=|5/2,-5/2\rangle$ hyperfine spin state [25]. The total atom number is $N\approx1.0\times10^5$ and the temperature is $T/T_F\approx0.3$, where T_F is the Fermi temperature of the trapped sample. The atoms are adiabatically loaded in a 2D optical lattice, which is formed by laser light with a wavelength of $\lambda_L=532$ nm in the xy horizontal plane. The lattice spacing and depth are $a_x=\lambda_L/2$ ($a_y=\lambda_L/\sqrt{3}$) and $V_{L,x}=5E_{L,x}$ ($V_{L,y}=20E_{L,y}$) along the x (y) direction, respectively, where $E_{L,x(y)}=[(\hbar^2\pi^2)/(2ma^2_{x(y)})]=h\times4.1(3.1)$ kHz and m is the atomic mass. Since the y-axis motion is frozen by the high lattice depth $V_{L,y}$ and the z-axis motion is irrelevant in the following experiment, our system is effectively 1D. Here, $k_L=\pi/a_x$ and the tunneling amplitudes are $\{t^r_0,t^r_1,t^r_2\}=h\times\{0.27,1.72,3.90\}$ kHz [26]. The trapping frequencies of the overall harmonic potential are estimated to be $\{\omega_x,\omega_y,\omega_z\}\approx2\pi\times\{64,49,135\}$ Hz. After loading the atoms in the lattice, the fractional population of the p orbital is less than 6%.

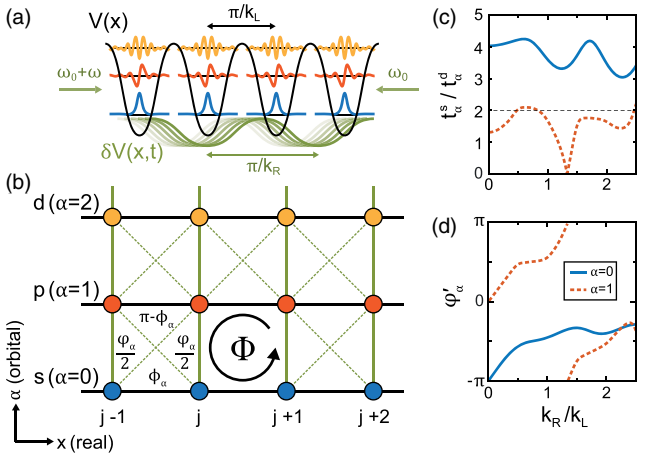

FIG. 1. Orbital-momentum coupling in an optical lattice. (a) Schematic of the experimental setup. Atoms are in a stationary 1D optical lattice potential $V(x)$, with lattice constant π/k_L, and driven by a moving lattice potential $\delta V(x,t)$, with lattice constant π/k_R. The moving lattice induces two-photon Raman transitions between the orbital states of the stationary lattice. (b) Ladder description of the system. The orbitals constitute the ladder legs along the real x dimension and the Raman coupling provides the interleg links. The complex coupling amplitude is spatially modulated, resulting in an effective magnetic flux per plaquette, $\Phi=2\pi(k_R/k_L)+\pi$. The subplaquette flux distribution is assigned in accordance with the cross-links indicated by the diagonal dashed green lines. (c) Amplitude ratio for the direct to diagonal hopping, t^s_α/t^d_α, and (d) their phase difference φ'_α as functions of k_R/k_L.

A moving lattice potential for interorbital Raman coupling is generated by a pair of 556 nm laser beams propagating in the xy plane, which is blue detuned by 1.97 GHz from the $^1S_0-{}^3P_1$ transition line. The wave number k_R of the moving lattice is determined by the x-axis projection of the relative wave vector of the two laser beams. Φ is controlled by the laser beam arrangement, and in this work, we employ two configurations, which correspond to $\Phi=1.48\pi$ and 2.44π, respectively [24]. The frequency difference ω for the two Raman beams is set to $\omega_c=[(\epsilon_1-2t^r_1)-(\epsilon_0-2t^r_0)]/\hbar=2\pi\times11.0$ kHz, matching the energy difference between the dispersion minima of the s and p bands. Under this condition, the coupling to orbitals higher than the d orbital is off resonance and the system can be approximated as a three-leg ladder consisting of s, p, and d orbitals.

The Bloch Hamiltonian of the three-leg ladder in momentum space is given by

$$H(q;\Phi)=\begin{pmatrix}\epsilon_0(q-\Phi) & \hbar\Omega_0(q)/2 & 0\\ \hbar\Omega_0(q)/2 & \epsilon_1(q)-\hbar\omega & \hbar\Omega_1(q)/2\\ 0 & \hbar\Omega_1(q)/2 & \epsilon_2(q+\Phi)-2\hbar\omega\end{pmatrix}, \quad (2)$$

where the α-orbital energy dispersion is $\epsilon_\alpha(q) = \epsilon_\alpha - 2t_\alpha^r \cos(q)$ and the α-$(\alpha+1)$ orbital coupling is $\hbar\Omega_\alpha(q) = t_\alpha^s - 2t_\alpha^d \cos(q + \alpha\varphi - \varphi'_\alpha)$. Here, q is quasimomentum normalized by a_x^{-1}. Figures 2(a) and 2(b) show the energy structures of the ladder system for our experimental conditions. The orbital-mixed ground band has a chiral region with only one pair of Fermi points, which is analogous to the chiral edge states in the integer quantum Hall effect [17,27]. We note that the cross-links of the ladder are manifested in the momentum dependence of $\Omega_\alpha(q)$. In particular, when $2t_\alpha^d > t_\alpha^s$, $\Omega_\alpha(q)$ changes its sign over a certain momentum range, implying that the topological character of the bands can change for a strong t_α^d. For the two cases of $\Phi = 1.48\pi$ and 2.44π, $\{t_0^s/t_0^d, t_1^s/t_1^d\}$ are estimated to be $\{4.2, 1.5\}$ and $\{4.2, 2.1\}$, respectively.

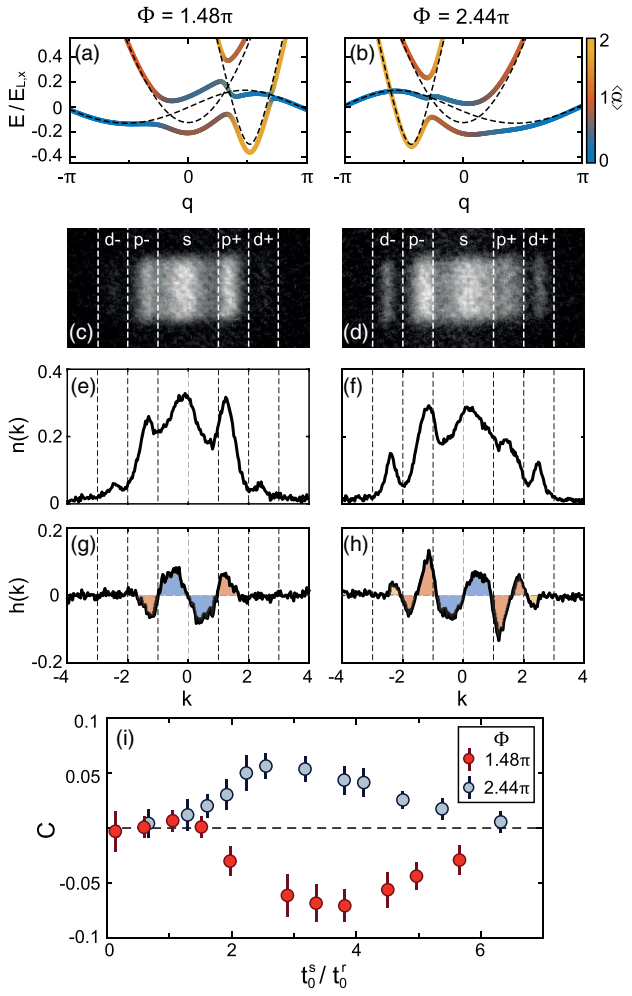

FIG. 2. Chiral currents in the fermionic three-leg ladder. Energy structures of the ladder system calculated from Eq. (2) for (a) $\Phi = 1.48\pi$ and $t_0^s/t_0^r = 3.4$ and (b) $\Phi = 2.44\pi$ and $t_0^s/t_0^r = 2.6$. The color indicates the mean orbital value $\langle\alpha\rangle$. The dashed lines show the bare band structures for zero interleg coupling. (c),(d) Band-mapped images of the samples for the parameter conditions in (a) and (b), respectively, and (e),(f) the corresponding 1D momentum distributions $n(k)$ obtained by integrating the images along the y direction. k is normalized by k_L. (g),(h) Asymmetry function $h(k) = n(k) - n(-k)$, demonstrating the chiral currents of the orbitals. (i) Evolution of $\mathcal{C} = J_0 - J_1$, where $J_\alpha = \int_\alpha^{\alpha+1} h(k)dk$, as a function of t_0^s/t_0^r. Each data point was obtained by averaging 20 measurements from the same experiment, with the error bar indicating the standard deviation of the measurements.

To probe the chirality of the ladder system, we load fermions in the orbital-mixed ground band and measure the momentum distributions of the orbitals. First, we turn on the Raman beams at the off-resonant frequency $\omega = \omega_c - 2\pi \times 6$ kHz and ramp ω to ω_c over 8 ms. The ramp time is limited by the scattering atom loss from the Raman beams, and in our loading process, the total atom number is reduced by 40%. The momentum distributions of the orbitals are measured using an adiabatic band-mapping technique [28]. After suddenly turning off the Raman beams, we linearly ramp-down the lattice potential to zero within 1 ms and, subsequently, take an absorption image of the atoms after a time of flight of 15 ms [Figs. 2(c) and 2(d)]. Here, the atoms in the α band are transferred to the αth Brillouin zone in the momentum space of free fermions; i.e., $\alpha < |k| < \alpha + 1$ (k is expressed in units of k_L). Integrating the measured 2D momentum distribution along the y direction, we obtain the 1D distribution $n(k)$ normalized as $\int n(k)dk = 1$ [Figs. 2(e) and 2(f)].

The chiral currents of the system are clearly observed from the asymmetric momentum distributions of the orbitals. The momentum asymmetry of the α band is quantified with $J_\alpha = \int_\alpha^{\alpha+1} h(k)dk$, where $h(k) = n(k) - n(-k)$ [Figs. 2(g) and 2(h)] [13,15]. Our measurements show $\{J_0, J_1, J_2\} = \{-0.049, 0.020, 0.002\}$ for $\Phi = 1.48\pi$ and $t_0^s = 3.4t_0^r$, and $\{J_0, J_1, J_2\} = \{0.037, -0.019, -0.008\}$ for $\Phi = 2.44\pi$ and $t_0^s = 2.6t_0^r$. The signs of the J_α's are consistent with the calculation results from the lowest bands in Figs. 2(a) and 2(b) [24]. We note that a nonzero chiral current exists in the middle leg because of the asymmetry between the edge legs with $t_0^r \neq t_2^r$ and $\Omega_0(q) \neq \Omega_1(q)$. In Fig. 2(i), we display the evolution of $\mathcal{C} = J_0 - J_1$ as a function of the relative interleg coupling, t_0^s/t_0^r. $|\mathcal{C}|$ initially increases as t_0^s/t_0^r increases, which is attributed to the gap opening, and it reaches a maximum at $t_0^s/t_0^r \sim 3$ before decreasing to zero for large t_0^s/t_0^r. In the limit of $t_0^s/t_0^r \to \infty$, the orbital states become fully mixed to suppress the chirality of the system [13,17,29].

Next, we investigate the quench dynamics of the ladder system to demonstrate the cross-link effect, wherein fermions are initially prepared in the s-orbital leg and the Raman beams are suddenly turned on at $\omega = \omega_c$. The sudden change of Ω_α will lead to a so-called skipping cyclotron motion along the ladder edge [13]. Recalling that the interorbital coupling strength is modulated as $\hbar\Omega_\alpha(q) = t_\alpha^s - 2t_\alpha^d \cos(q + \alpha\varphi - \varphi'_\alpha)$, we expect that the cross-link effect can be directly revealed by a momentum-resolved

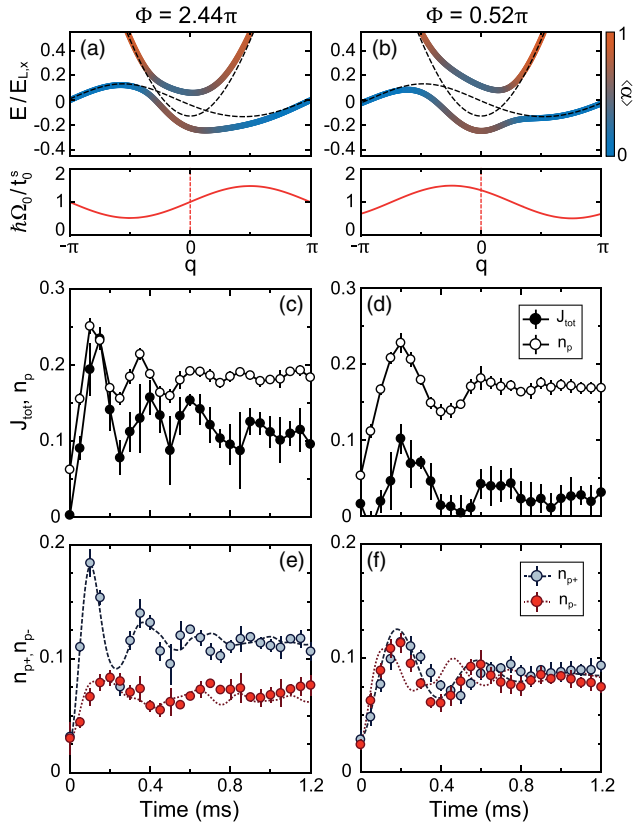

FIG. 3. Quench dynamics of the ladder system and effects of the complex cross-links. Energy structures of the $s-p$, two-leg ladder, and the interleg coupling strength $\hbar\Omega_0(q)/t_0^s$ for (a) $\Phi = 2.44\pi$ and (b) $\Phi = 0.52\pi$. Here, $t_0^s/t_0^r = 4$ for clear indication of the effect of the momentum dependence of $\Omega_0(q)$. Atoms are initially prepared in the s band and quench dynamics is initiated by suddenly turning on the interleg coupling. Time evolutions of the total momentum asymmetry $J_{\text{tot}} = J_0 + J_1 + J_2$ and the p-band fractional population n_p for (c) $\Phi = 2.44\pi$ and $t_0^s/t_0^r = 11.3$ and (d) $\Phi = 0.52\pi$ and $t_0^s/t_0^r = 8.5$. (e),(f) Corresponding time evolutions of $n_{p\pm} = \int_{\pm 1}^{\pm 2} n(k,t)dk$. The different oscillation periods for $n_{p\pm}$ reflect the modulations of $\Omega_0(q)$. Each data point was obtained from seven measurements and its error bar denotes the standard deviation. Dashed and dotted lines show the numerical results of n_{p+} and n_{p-}, respectively.

analysis of the quench dynamics. We examine two cases, $\Phi = 2.44\pi$ and 0.52π, which show almost the same effective magnetic flux $\sim\pi/2$ in a modulus of 2π but different modulation phases of $\Omega_0(q)$ with $\varphi_0{}' = -0.5\pi$ and 0.75π, respectively [Figs. 3(a) and 3(b)]. In the case of $\Phi = 2.44\pi$ (0.52π), the average coupling strength for $q > 0$, $\langle\Omega_0\rangle_+$, is stronger (weaker) than that for $q < 0$, $\langle\Omega_0\rangle_-$, so the p-band population with positive momentum will show faster (slower) oscillations than that with negative momentum. Here, the case of $\Phi = 0.52\pi$ is generated by reversing the Raman beam directions from those for $\Phi = 1.48\pi$, i.e., $k_R \to -k_R$.

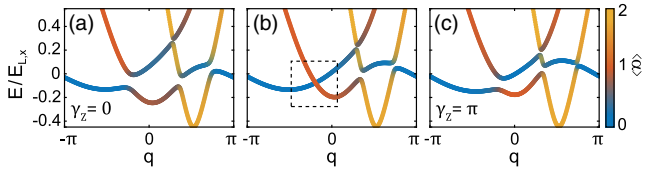

FIG. 4. Topological phase transition of the three-leg ladder system. Band dispersion of the system for (a) $t_0^s/t_0^d = 2.5$, (b) 1.15, and (c) 0 with $\{k_R/k_L, t_0^d/t_0^r, t_1^s/t_0^r, t_1^d/t_0^r, \varphi_0', \varphi_1'\} = \{0.24, 1.5, 6.1, 3.6, -\pi/2, \pi/2\}$. The Zak phase of the ground band changes from $\gamma_Z = 0$ in (a) to $\gamma_Z = \pi$ in (c). The topological phase transition is featured with a gap closing in the boxed region in (b).

The time evolution of the total momentum asymmetry $J_{\text{tot}} = \sum_\alpha J_\alpha$ and the p-band population n_p are shown in Figs. 3(c) and 3(d). The in-phase oscillations for J_{tot} and n_p are consistent with the skipping motion expected under a magnetic flux [30]. The corresponding time evolution of the p-band populations with positive and negative momenta, $n_{p\pm}(t) = \int_{\pm 1}^{\pm 2} n(k,t)dk$, are shown in Figs. 3(e) and 3(f). We observe that n_{p+} oscillates faster (slower) than n_{p-} for $\Phi = 2.44\pi$ ($\Phi = 0.52\pi$), as expected from the momentum dependence of $\Omega_0(q)$. The oscillation time difference is characterized by $\eta = \tau_{p-}/\tau_{p+}$, where $\tau_{p\pm}$ is the time at which the first oscillation minimum occurs in $n_{p\pm}(t)$. Our measurements give $\eta = 1.92$ and 0.81 for $\Phi = 2.44\pi$ and 0.52π, respectively, which are found to be well accounted for by the average coupling strength ratio $\langle\Omega_0\rangle_+/\langle\Omega_0\rangle_- = (\pi t_0^s - 4t_0^d \sin\varphi_0')/(\pi t_0^s + 4t_0^d \sin\varphi_0') = 1.9$ and 0.7 for $\Phi = 2.44\pi$ and 0.52π, respectively. We also observe that the numerical simulations based on Eq. (2) show reasonable agreement with the experimental data.

Finally, we discuss the topological phase transition of the cross-linked chiral ladder system, which is anticipated to occur with an increasing cross-link strength [16–19]. We calculate the Zak phase γ_Z of the orbital-mixed ground band over the parameter space of our ladder system and identify multiple regions of topologically nontrivial phases with $\gamma_Z \neq 0$ for $t_0^s/t_0^d < 2$ (Fig. 4) [24,31]. As a means of controlling the strength and phase of the complex cross-link, it is conceivable in experiment to tailor the orbital wave functions by engineering lattice potential [32]. We note that the $p-d$ orbital coupling in our system has $t_1^s/t_1^d \approx 1.5 < 2$ for $\Phi = 1.48\pi$, highlighting the significant role of the orbital wave functions in determining the link properties.

In conclusion, we realized a cross-linked chiral fermionic ladder based on the orbital states of a 1D optical lattice. The chiral edge currents were observed and the cross-link effect was demonstrated by the momentum dependence of the interorbital coupling strengths. The orbital-based synthetic ladder system has an explicitly broken leg symmetry with $t_\alpha^r \neq t_\beta^r$, providing an interesting opportunity for studying topological phases protected by

unconventional symmetries [10,33]. Our orbital-momentum coupling scheme can be extended to multiple hyperfine spin states, which would allow for interactions between fermions [34].

This work was supported by the Institute for Basic Science in Korea (Grant No. IBS-R009-D1) and the National Research Foundation of Korea (Grants No. NRF-2018R1A2B3003373 and No. 2014-H1A8A1021987).

*yishin@snu.ac.kr

[1] X. G. Wen, Topological orders in rigid states, Int. J. Mod. Phys. B **4**, 239 (1990).
[2] M. Z. Hasan and C. L. Kane, Colloquium: Topological insulators, Rev. Mod. Phys. **82**, 3045 (2010).
[3] N. Goldman, G. Juzeliūnas, P. Öhberg, and I. B. Spielman, Light-induced gauge fields for ultracold atoms, Rep. Prog. Phys. **77**, 126401 (2014).
[4] D. Jaksch and P. Zoller, The cold atom Hubbard tool box, Ann. Phys. (Amsterdam) **315**, 52 (2005).
[5] I. Bloch, J. Dalibard, and W. Zwerger, Many-body physics with ultracold gases, Rev. Mod. Phys. **80**, 885 (2008).
[6] M. Aidelsburger, M. Atala, M. Lohse, J. T. Barreiro, B. Paredes, and I. Bloch, Realization of the Hofstadter Hamiltonian with Ultracold Atoms in Optical Lattices, Phys. Rev. Lett. **111**, 185301 (2013).
[7] H. Miyake, G. A. Siviloglou, C. J. Kennedy, W. C. Burton, and W. Ketterle, Realizing the Harper Hamiltonian with Laser-Assisted Tunneling in Optical Lattices, Phys. Rev. Lett. **111**, 185302 (2013).
[8] G. Jotzu, M. Messer, R. Desbuquois, M. Lebrat, T. Uehlinger, D. Greif, and T. Esslinger, Experimental realization of the topological Haldane model with ultracold fermions, Nature (London) **515**, 237 (2014).
[9] A. Altland and M. R. Zirnbauer, Nonstandard symmetry classes in mesoscopic normal-superconducting hybrid structures, Phys. Rev. B **55**, 1142 (1997).
[10] B. Song, L. Zhang, C. He, T. F. J. Poon, E. Hajiyev, S. Zhang, X.-J. Liu, and G.-B. Jo, Observation of symmetry-protected topological band with ultracold fermions, Sci. Adv. **4**, eaao4748 (2018).
[11] O. Boada, A. Celi, J. I. Latorre, and M. Lewenstein, Quantum Simulation of an Extra Dimension, Phys. Rev. Lett. **108**, 133001 (2012).
[12] A. Celi, P. Massignan, J. Ruseckas, N. Goldman, I. B. Spielman, G. Juzeliūnas, and M. Lewenstein, Synthetic Gauge Fields in Synthetic Dimensions, Phys. Rev. Lett. **112**, 043001 (2014).
[13] M. Mancini, G. Pagano, G. Cappellini, L. Livi, M. Rider, J. Catani, C. Sias, P. Zoller, M. Inguscio, M. Dalmonte, and L. Fallani, Observation of chiral edge states with neutral fermions in synthetic Hall ribbons, Science **349**, 1510 (2015).
[14] B. K. Stuhl, H.-I. Lu, L. M. Aycock, D. Genkina, and I. B. Spielman, Visulaizing edge states with an atomic Bose gas in the quantum Hall regime, Science **349**, 1514 (2015).
[15] L. F. Livi, G. Cappellini, M. Diem, L. Franchi, C. Clivati, M. Frittelli, F. Levi, D. Calonico, J. Catani, M. Inguscio, and L. Fallani, Synthetic Dimensions and Spin-Orbit Coupling with an Optical Clock Transition, Phys. Rev. Lett. **117**, 220401 (2016).
[16] M. Creutz, End States, Ladder Compounds, and Domain-Wall Fermions, Phys. Rev. Lett. **83**, 2636 (1999).
[17] D. Hügel and B. Paredes, Chiral ladders and the edges of quantum Hall insulators, Phys. Rev. A **89**, 023619 (2014).
[18] J. Jünemann, A. Piga, S.-J. Ran, M. Lewenstein, M. Rizzi, and A. Bermudez, Exploring Interacting Topological Insulators with Ultracold Atoms: The Synthetic Creutz-Hubbard Model, Phys. Rev. X **7**, 031057 (2017).
[19] N. Sun and L.-K. Lim, Quantum charge pumps with topological phases in a Creutz ladder, Phys. Rev. B **96**, 035139 (2017).
[20] X. Li, E. Zhao, and W. V. Liu, Topological states in a ladder-like optical lattice containing ultracold atoms in higher orbital bands, Nat. Commun. **4**, 1523 (2013).
[21] S.-L. Zhang and Q. Zhou, Shaping topological properties of the band structures in a shaken optical lattice, Phys. Rev. A **90**, 051601 (2014).
[22] M. A. Khamehchi, C. Qu, M. E. Mossman, C. Zhang, and P. Engels, Spin-momentum coupled Bose-Einstein condensates with lattice band pseudospins, Nat. Commun. **7**, 10867 (2015).
[23] O. Dutta, M. Gajda, P. Hauke, M. Lewenstein, D.-S. Lühmann, B. A. Malomed, T. Sowiński, and J. Zakrzewski, Non-standard Hubbard models in optical lattices: A review, Rep. Prog. Phys. **78**, 066001 (2015).
[24] See Supplemental Material at http://link.aps.org/supplemental/10.1103/PhysRevLett.121.150403 for the details of the tight-binding model, the experimental setup and sequence, and the Zak phase calculation.
[25] M. Lee, J. H. Han, J. H. Kang, M.-S. Kim, and Y. Shin, Double resonance of Raman transitions in a degenerate Fermi gas, Phys. Rev. A **95**, 043627 (2017).
[26] J. Heinze, S. Götze, J. S. Krauser, B. Hundt, N. Fläschner, D.-S. Lühmann, C. Becker, and K. Sengstock, Multiband Spectroscopy of Ultracold Fermions: Observation of Reduced Tunneling in Attractive Bose-Fermi Mixtures, Phys. Rev. Lett. **107**, 135303 (2011).
[27] C. L. Kane, R. Mukhopadhyay, and T. C. Lubensky, Fractional Quantum Hall Effect in an Array of Quantum Wires, Phys. Rev. Lett. **88**, 036401 (2002).
[28] M. Köhl, H. Moritz, T. Stöferle, K. Günter, and T. Esslinger, Fermionic Atoms in a Three Dimensional Optical Lattice: Observing Fermi Surfaces, Dynamics, and Interactions, Phys. Rev. Lett. **94**, 080403 (2005).
[29] E. Cornfeld and E. Sela, Chiral currents in one-dimensional fractional quantum Hall states, Phys. Rev. B **92**, 115446 (2015).
[30] The dephasing timescale of oscillation was about 1 ms, which is attributed to the averaged dynamics from different initial states [13] and fluctuations of the relative phase of the Raman beam pair.

[31] J. Zak, Berry's Phase for Energy Bands in Solids, Phys. Rev. Lett. **62**, 2747 (1989).

[32] B. Liu, X. Li, and W. V. Liu, Topological phases via engineered orbital hybridization in noncentrosymmetric optical lattices, Phys. Rev. A **93**, 033643 (2016).

[33] J.-M. Hou, Hidden-Symmetry-Protected Topological Semimetals on a Square Lattice, Phys. Rev. Lett. **111**, 130403 (2013).

[34] S. Barbarino, L. Taddia, D. Rossini, L. Mazza, and R. Fazio, Synthetic gauge fields in synthetic dimensions: Interactions and chiral edge modes, New J. Phys. **18**, 035010 (2016).